Experimental and numerical investigation of the thermal inertia of sugar-beet-pulp/starch based bricks enhanced with phase change materials

Martin Tenpierik, Mohammed Lachi, Christophe Bliard, Guillaume Polidori, Chadi Maalouf

Experimental and numerical investigation of the thermal inertia of sugar-beet-pulp/starch based bricks enhanced with phase change materials

Martin J. Tenpierik[1], Mohammed Lachi[2], Christophe Bliard[3], Guillaume Polidori[2], Chadi Maalouf[2]*

[1] Department of Architectural Engineering and Technology, Faculty of Architecture and the Built Environment, Delft University of Technology, Julianalaan 134, 2628BL Delft, the Netherlands, email: m.j.tenpierik@tudelft.nl

[2] Laboratoire de MATériaux et Ingénieurie Mécanique, MATIM, University of Reims-Champagne-Ardenne, URCA, Moulin de la Housse, 51687 Reims Cedex 2, France

[3] Institut de Chimie Moléculaire de Reims, ICMR-UMR 7312 CNRS, University of Reims-Champagne-Ardenne, URCA, Moulin de la Housse, 51687 Reims Cedex 2, France

[*] Corresponding author.

Abstract

Due to environmental concerns, bio-based materials are being increasingly investigated and used in buildings. In general, the density of these materials, and thus their thermal inertia, is low. Thermal inertia can be beneficial for reducing the energy use of buildings by damping indoor temperature fluctuations or by reducing and delaying incoming (solar) heat through the façade.

This study explores the thermal inertia of regular-sized bricks made of a sugar-beet-pulp/starch mixture (BP/S), and with 17 circular holes inside. The holes were filled either with the BP/S mixture, with air, with a stabilised phase change material (PCM) gel or with a salt-hydrate based PCM. The brick was insulated on all sides but one. Two series of experimental measurements were performed: 1.) a heating film placed at the back (insulated) side of the brick heated the brick until steady-state conditions were reached; 2.) the heated brick was then passively cooled down to ambient temperature by cutting the power to the heating film. Numerical simulations of these experimental measurements were also modelled using the COMSOL Multiphysics® software. In addition, simulations were run to study the thermal inertia of a full brick wall made out of 1 layer and of 4 layers of the BP/S brick with and without PCM, exposed to a combination of a sinusoidal outdoor air temperature fluctuation with an imposed radiation flux on the outdoor surface, representing summer conditions.

The results show that the brick in which the holes were filled with phase change material had a slower temperature response and thus higher thermal inertia than the bricks in which the holes were filled with BP/S or with air. The salt-hydrate based PCM with the higher latent heat of fusion led to the slowest

temperature response and highest thermal inertia. Furthermore, the calculated simulations could accurately reproduce the experimental measurements. Applying PCM in thick walls (40 cm) made of BP/S bricks however hardly affects the temperature amplitude damping and time delay of the complete wall. The addition of PCM therefore is only effective for thinner walls (10 cm).

Keywords: beet-pulp, starch, phase change material, hollowed brick, thermal inertia, experiment, simulation

1. Introduction

Because of climate change, scarcity of fossil energy resources, geopolitics and international treaties, many countries currently undergo an energy transition in which fossil energy resources are being replaced by sustainable and renewable energy sources. In the European Union in 2020, households and the commercial and public services sector accounted for around 42% of the total final energy consumption [1]. As part of the energy transition, a large challenge lies in reducing the final energy consumption of buildings, towards nearly or net zero energy buildings or even energy positive buildings. Thermally well-insulated building envelopes and the thermal mass of construction materials play an important role in reaching Europe's targets. Under summer conditions, facades with high thermal mass will dampen the temperature amplitude and create a time delay of incoming heat induced on the façade by solar radiation, thereby reducing the cooling demand of the building.

Furthermore, the architecture, engineering, and construction (AEC) sector is responsible for a large share in the extraction of raw materials for building materials [2]. In December 2015, the European Commission [3] adopted the Circular Economy Action Plan, which aims to move the EU into a climate-neutral, competitive, circular economy. One of the key elements is to turn waste into resources. Concerning the circular economy, the Ellen MacArthur Foundation [4] defines two different cycles: one for renewables and one for finite materials. In this light, bio-sourced construction materials and/or construction materials that make use of agricultural waste are increasingly investigated in the research community. Besides, their application in the AEC industry is increasing.

Recently, several studies into the mechanical and building physical properties of bio-based materials for buildings have been conducted. For example, Maalouf et al. [5] explored the use of hempcrete as a building envelope material in three French cities under summer conditions. They among others concluded that the thermal inertia of the hempcrete was lower than that of concrete and suggested combining hempcrete with a material with higher thermal mass to increase the temperature amplitude

damping and the time delay of the façade for incoming solar heat. Collet et al. [6] further investigated the thermal properties of different mixtures of hempcrete and observed that density had an important impact on the thermal conductivity. The transient hygro-thermal behaviour of the material as part of a wall assembly was studied by Colinart et al. [7]. Besides hempcrete, other bio-sourced materials have been investigated too. Haba et al. [8], for instance, studied date palm concrete and concluded that this bio-composite had similar hygroscopic sorption characteristics to hemp-lime. Recently, an alternative bio-based building material based on sugar-beet-pulp and potato starch (BP/S) caught the attention of researchers who explored its hygro-thermal [9, 10, 11], acoustical [9, 10] and mechanical properties [11]. They found that a starch-beet pulp mass ratio of 0.4 led to the most favourable properties of this material for application in buildings. However, several studies concluded that due to a low density many bio-based alternatives presented low thermal inertia as compared to concrete or clay bricks.

In order to increase the thermal inertia of bio-based bricks made from for instance hempcrete or BP/S, phase change materials (PCMs) could be advantageously used. PCMs can latently store/release a significant amount of heat during the phase transition without a significant change in temperature. This property makes them interesting for application in lightweight buildings or lightweight construction materials with low thermal inertia. The application of PCMs in buildings and their facades has been explored or reviewed already by many researchers. Gutherz and Schiler [12] for example looked into their use as a means of passive solar heating in the façade. Weinläder et al.[13] and Goia et al. [14] considered their application for passive heating and daylighting. Tyagi and Buddhi [15], Baetens at al. (16], Kalnaes and Jelle [17] and Bland et al. [18] reviewed the literature on their application in buildings. And Fiorito [19], Wang and Zhao [20] and Tenpierik et al. [21, 22], among others, considered their application in Trombe walls or curtains behind glass. However, only a limited number of studies on the use of PCMs in bricks for facades have been conducted. For example, Wang et al. [23] investigated PCM enhanced mortar bricks in a full-scale test set-up of an exterior wall in Shanghai and compared the wall's performance to a wall made of perforated vitrified bricks. They found that in summer the PCM containing wall led to a reduction of about 0.2 ^{o}C for the maximum temperature on the inside surface of the wall and a thermal time delay of about 1 to 2 hours, in total resulting in a 24% reduction of the cooling load. Laaouatni et al. [24, 25] explored the combination of hollow concrete blocks with a stabilised PCM gel and internal ventilation channels. With experiments and simulations, they showed that such a system enables better control of the storage and release of heat. Sawadogo et al. [26] characterised the hygrothermal properties of a mixture of PCM with hemp concrete for passive energy storage in buildings. They only looked into the materials properties and not into a potential application

as bricks in facades. In 2023, Canim and Kalfa [27] studied the integration of paraffin based PCM into a pumice block for façade applications. They concluded that the thermal inertia of the pumice block increased by 75% when it was filled with 15% PCM.

This study uses COMSOL Multiphysics® to explore the thermal inertia of bio-sourced bricks and walls. COMSOL Multiphysics® is a multiphysics, multi-solver, finite element analysis package that has been used before to study the thermal inertia of buildings and building materials. Recently, Alayed et al. [28], for example, used it to study the impact of sensible thermal mass on the energy consumption of buildings in hot climates. Johra et al. [29] used it as one of the methods for exploring the effect of the thermal inertia of PCMs (without hysteresis) on energy flexibility of the heating demand of buildings. Frei [30] and Rubinetti et al. [31] did first studies into the modelling of thermal hysteresis of PCMS with the software.

So far, there have been no studies on the integration of PCMs in lightweight bio-based construction products, such as bricks. The present study therefore explores how the thermal inertia of a lightweight hollow brick made of a mixture of sugar beet pulp and starch can be increased by integrating a stabilised gel-based PCM. Furthermore, the effect of salt-hydrate based addition and PCM with higher latent heat enthalpy inclusion on the thermal inertia was studied as well. This study compares both experimental measurements and direct numerical simulations using the COMSOL Multiphysics® Software to explore the thermal inertia of one brick. In addition, COMSOL Multiphysics® Software was used to study the thermal inertia of a full brick wall made out of one layer and of four layers of the bio-sourced brick with and without PCM.

2. Materials and Methods

This study consists of two parts. Part I is an experimental study that on the one hand was used to validate the simulations performed in part II, and on the other hand adds an understanding of how the thermal inertia of lightweight bio-based materials can be increased by including phase change materials. Part II is a simulation-based study that further investigates and supports the findings of the experimental study.

2.1 Materials and material properties

Based on Karaky's thesis work [9, 10], which studied the optimal composition of BP/S from a mechanical, acoustical, and hygrothermal properties point of view, the ratio of 40% of potato starch with respect to the total pulp mass was selected to be used in the present work. First beet-pulp pellets

obtained from Cristal Union were soaked separately for two hours in distilled water to reach their saturation degree with a mass ratio of water/pulp equal to 2.5. Then, potato starch powder (from Roquette) was added to the saturated pulps and they were mixed manually for 10 minutes until a homogeneous admix was obtained. The obtained mixture was then placed in an autoclave and heated for 30 minutes at 120 °C to obtain a heterogeneous gel. The resulting gel was poured into wooden moulds (Figure 1) and compacted under a pressure of 0.044 MPa. The obtained specimens were frozen and dried by lyophilisation as shown in Constantine et al. [11]. Figure 2 shows a brick sample after drying.

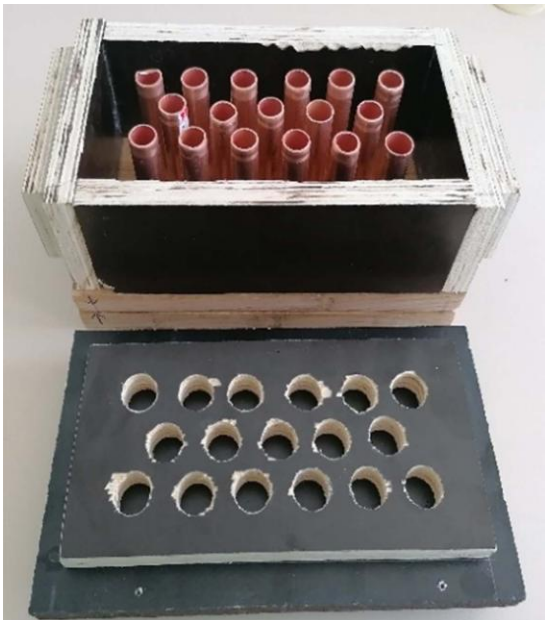

Figure 2: Mold used for brick manufacturing

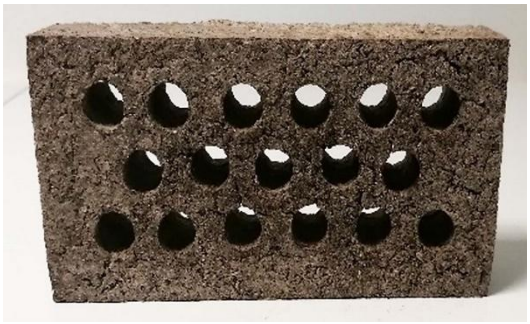

Figure 1: Brick sample after drying

Figure 3*: Brick sample filled with PCM1*

Figure 4 shows the dimensions of one brick: 218.5 mm in length, 103.0 mm in width, and 56.0 mm in height. It contains 3 rows of holes: 2 rows of 6 holes and 1 row of 5 holes. The radius of these holes is 8.5 mm. The dry material had a thermal conductivity of 0.075 $W \cdot m^{-1} \cdot K^{-1}$ [9], a density of 360 $kg \cdot m^{-3}$ [9, 11] and specific heat of around 1400 $J \cdot kg^{-1} \cdot K^{-1}$ [9]. For this research, the holes were either filled with BP/S, still air (figure 2), granular encapsulated PCM (PCM1) (figure 3) or a salt-hydrate PCM (PCM2). Both simulations and measurements investigate this material as an example of a bio-sourced construction material.

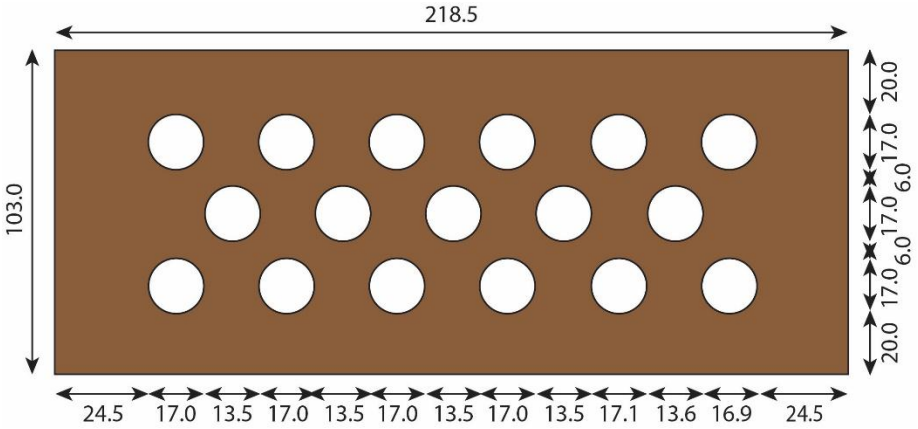

Figure 4: Cross section through the BP/S brick. Dimensions in mm. Height of the brick is 56.0 mm.

PCM1 is a granular polyolefin elastomer (a stabilised PCM resin made of 40 % ethylene copolymer and 60 % paraffin wax) with a phase change centred around 22.1 °C during the heating cycle and 18.2 °C during the cooling cycle. The enthalpy curve was measured by DSC using a 2 $K.min^{-1}$ heating rate (Figure 5a). The PCM is considered incompressible which means that the enthalpy only depends on temperature. The latent heat was modelled as part of the specific heat, c_p, for which the data from the manufacturer was used (Figure 5b). The density of the PCM was assumed to be 813 $kg.m^{-3}$ based on data specified by the manufacturer. Besides, the PCM was modelled as a solid because the material has a solid-solid phase change in the relevant temperature range. The PCM is a gel encapsulated in small grains as a result of which no fluid flow will take place. The thermal conductivity of the PCM1 was estimated to be around 0.2 $W.m^{-1}.K^{-1}$. In the simulations, the opacity of the PCM on the ambient spectral band was set to opaque because of its limited transparency in this spectral band.

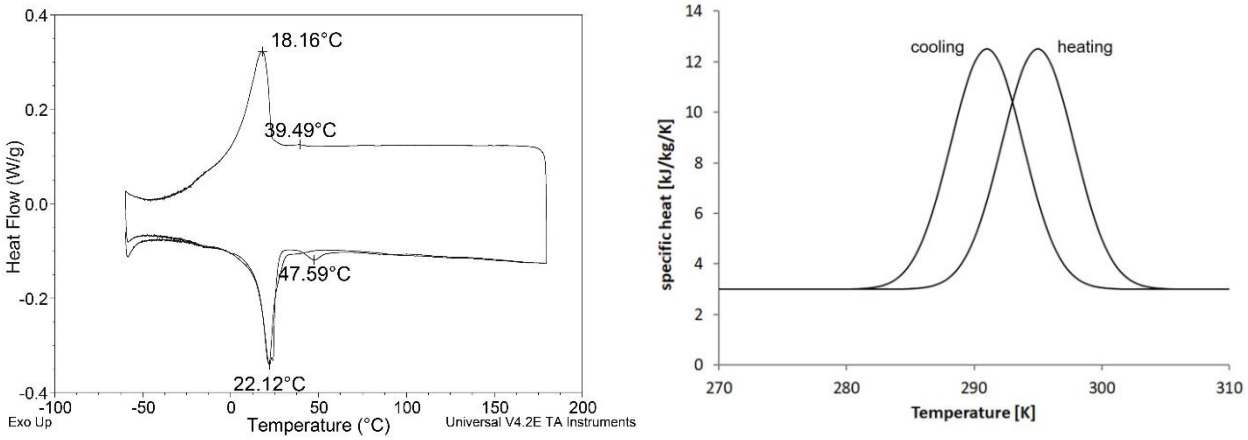

Figure 5: Results of DSC measurements on PCM1 (a) and Specific heat of PCM1 for the heating and cooling cycle (b).

PCM2, only used in the simulations, is a salt-hydrate with a phase change centred around 25 °C during the melting process and 24 °C during the solidification process. As specified by the manufacturer, the density of the PCM was 1500 kg.m^{-3} in the solid state and 1400 kg.m^{-3} in the liquid state (modelled as continuous second derivative smoothing with an absolute size transition zone of 4 °C centred around the phase change temperature). From 27°C and up the PCM follows a similar change in density as seen in water. The density was therefore modelled as a temperature dependent variable with a density as shown in Figure 6a. According to the manufacturer, the latent heat of the PCM was 180 kJ.kg^{-1} within a temperature range from 17 °C to 32 °C. The sensible specific heat equals 2 kJ.kg^{-1}.K^{-1}. The latent heat was modelled as part of the specific heat, c_p, by raising this value from 2 kJ.kg^{-1}·K^{-1} to a value that was specified by the manufacturer (Figure 6b). Besides, the PCM was modelled as a liquid with a temperature dependent dynamic viscosity. The viscosity was chosen high (1.10^{4} Pa.s) for the solid state as a result of which the modelled liquid behaved as a solid in that state. The liquid state of the PCM had a dynamic viscosity of 1.10^{-2} Pa.s as a result of which it behaved as a liquid in that state (modelled as continuous second derivative smoothing with an absolute size transition zone of 4 °C). The thermal conductivity of the PCM 2 was assumed constant at 0.6 W.m^{-1}.K^{-1} within the relevant temperature range. The opacity of the PCM on the ambient spectral band was set to opaque in the simulations. The properties and simulation settings of this PCM were validated in a previous study by Tenpierik et al. [22].

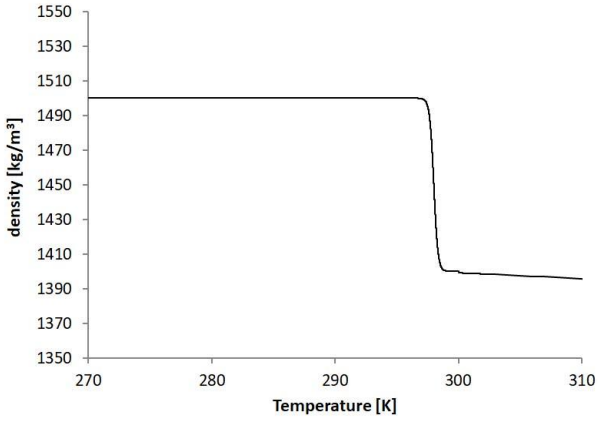

Figure 6a: Density of PCM2 for the heating cycle.

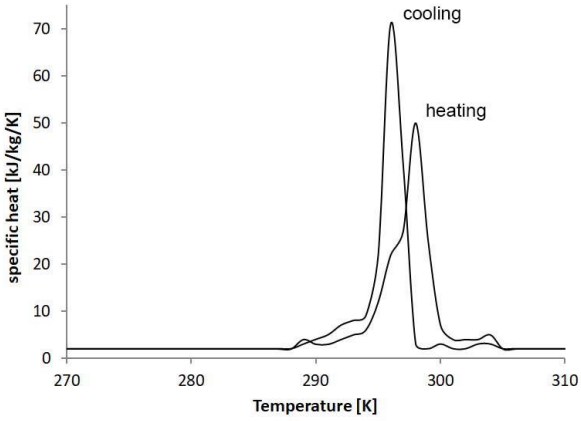

Figure 6b: Modelled specific heat of PCM2 for the heating and cooling cycle.

Property	PCM1	PCM2
Phase change temperature heating / cooling cycle [^{o}C]	22.1 / 18.2	25 / 24
Density solid / liquid [kg.m^{-3}]	813 / 813	1500 / 1400

thermal conductivity [$W.m^{-1}.K^{-1}$]	0.2	0.6
(Latent) enthalpy [$kJ.kg^{-1}$]	118 (14-30 ^{o}C)	180 (17-32 ^{o}C)
Specific heat [$kJ{\cdot}kg^{-1}{\cdot}K^{-1}$]	3	2

Table 1: overview of the properties of the used PCMs.

2.2 Part I: experimental measurements

The experimental setup consists of the brick with or without PCM equipped with thermocouples, flux meters, a heating film on the brick back face, a data logger and a computer (figures 7a, b and c). In figure 7c is presented only a view of the brick with holes filled by PCM.

Figure 7a: Current generation system for the heating film.

Figure 7b: All the equipment making up the experimental measurement chain: sample, acquisition unit and computer.

Figure 7c: View of the brick with holes filled by PCM.

All faces of the brick were insulated using an insulation plastic foam material, except for the front facing ambient air. This front face was instrumented by two thin heat flux meters (from Captec) and a surface thermocouple. Another thermocouple was kept at a distance from the surface in the ambient air. Thermocouples type K and J, which were all calibrated before use, were also placed on the surface of the heating film (figure 8), inside three of the holes (figure 7c) and on the back and side surfaces of the test set-up. Figures 9 and 10 give an overview of the positioning of the sensors in the brick and on the heating film.

The heating film (figure 8) was placed on the back face of the brick (see figures 9 and 10) and is connected to a constant current heat-generating source allowing the film to generate a uniform power heat flux on its entire surface. The heating power supplied by the system was 182 $W.m^{-2}$ over the entire surface of the heating film (= 25 V * 0.089 A / (0.056 m x 0.218 m)). For the measurement of temperatures and voltages, the data logger MIDI DATA LOGGER GL840 SERIES from Graphtec was used [https://www.graphtecamerica.com]. Table 2 provides an overview of the inaccuracies of the equipment.

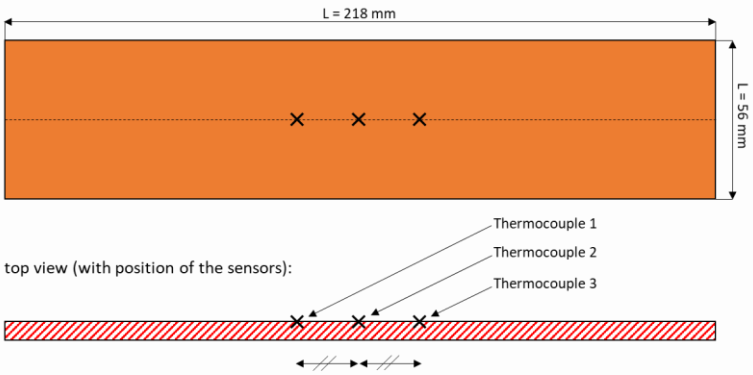

Figure 8: horizontal and vertical view of the heating film.

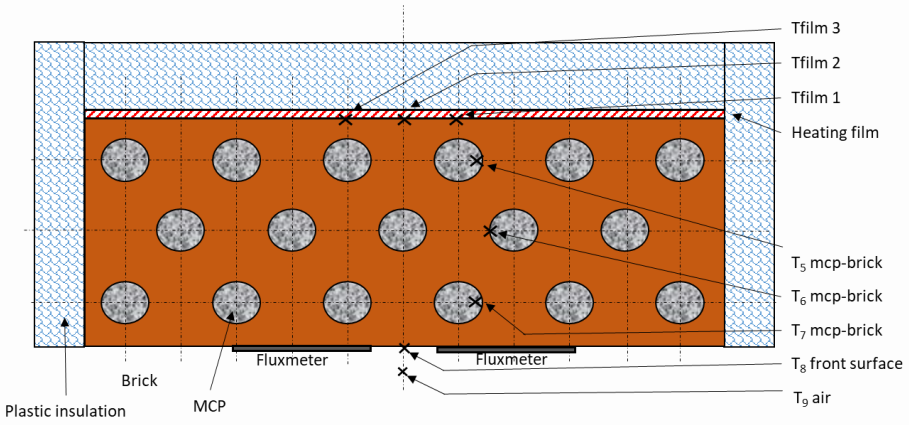

Figure 9: Schematic diagram of thermocouples positions.

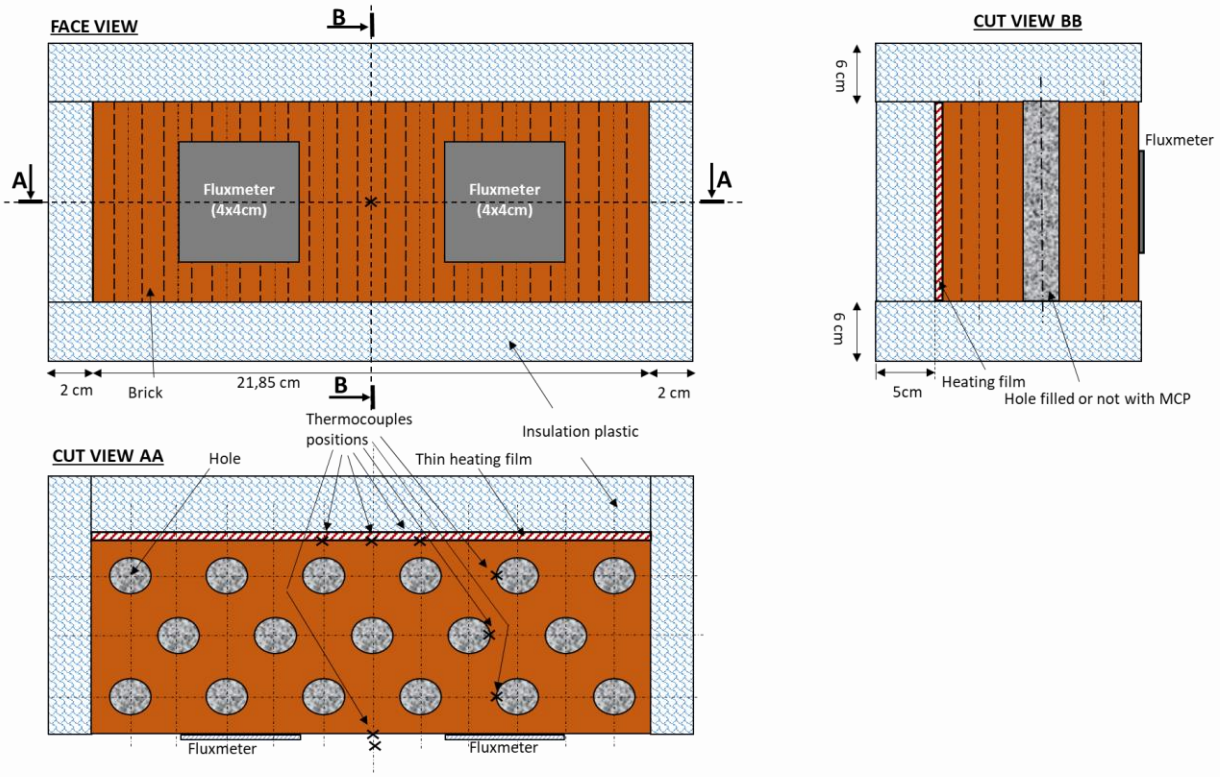

Figure 10: Sketch of the experimental setup. Face view and horizontal (cut AA) and vertical (cut BB) cross sections view through the measurement set-up.

Thermocouple	Measurement Range	Measurement Accuracy

K	- 100 < T ≤ 1370 ℃	± 0.8 ℃
T	-100 < T < 400 °C	± 0.6 °C
J	-100 < T < 100 °C	± 0.8 °C
Voltage		± (0.05 % of F.S. + 10µV)

Table 2: overview of inaccuracies of the equipment.

The experimental measurements were conducted on the bricks with the holes being filled with either BP/S material, with air or with PCM1 (figure 7c). A period of three days was set between each series of measurements to allow the brick to return to ambient air conditions. Furthermore, both the heating and cooling process were investigated. An overview of the experimental measurements is presented in table 3.

Hole filling	BP/S	air	PCM1
Heating phase: V = 25 V, I = 89 mA	MEAS1.bp/s	MEAS1.air	MEAS1.pcm1
Passively cooling down: V = 0 V, I= 0 mA	MEAS2.bp/s	MEAS2.air	MEAS2.pcm1

Table 3: overview of different simulations.

During the heating phase, a constant heat flux was imposed on the entire backside of the brick from time t = 0 till time t = t_1. Then the power supply of the heating film was stopped so that the heating power was set to 0 $W.m^{-2}$; then from t = t_1 until t = t_{end} the cooling process commenced. During the whole time frame the temperature changes were recorded over time.

2.3 Part II: brick level simulations: simulation model and settings

Numerical simulations were performed using the COSMOL Multiphysics® Software in order to model the thermal properties of the studied specimens. The calculated simulations allowed to look into the 3D thermal performances of such bricks. The model was set-up parametrically meaning that the dimensions of the bricks, the radius of the holes and the number of holes per row and the number of rows could be controlled easily by simply changing one parameter; hence allowing to investigate more easily different configurations in the future.

For air, the built-in properties in COMSOL were used, except for the thermal conductivity. In order to simplify the simulations, this latter value was modified to also include the effect of IR radiation exchange between the surfaces around the holes. Based on a surface emissivity of 0.9 in the IR spectral band and

a hole radius of 8.5 mm, an effective thermal conductivity of 0.067 $W.m^{-1}.K^{-1}$ was determined. For the other materials, the properties mentioned in section 2.1 were used.

Simulations were performed to corroborate the results from the experiments. The same series of simulations were run as explained in the previous section on experiments with the power of the heating film and the temperature of the surrounding air as inputs to the model. These conditions were applied to the simulations on the specimens with holes filled with BP/S, air or PCM1. The same conditions were also used to simulate additional variants in which the holes were filled with PCM2 to understand whether a salt-hydrate with higher latent heat capacity within a narrow temperature range provides additional thermal inertia. The same power and temperature as for the PCM1 case were used as initial and boundary conditions. An overview of the simulations is presented in table 4 below.

Hole filling	BP/S	air	PCM1	PCM2
Heating phase: V = 25 V, I = 89 mA	SIM1.bp/s	SIM1.air	SIM1.pcm1	SIM1.pcm2
Passively cooling down: V = 0 V, I = 0 mA	SIM2.bp/s	SIM2.air	SIM2.pcm1	SIM2.pcm2

Table 4: overview of different simulations.

For all simulations, the heat transfer in solids and fluids physics modules of COMSOL version 5.6 were used. Fluid flow (creeping flow) was also included for the PCM2, which has a solid-liquid phase change. Creeping flow in that case was selected because after some initial tests the flow of the molten PCM had a low speed and therefore a low Reynolds number. The simulations were based on a transient scheme of a 3D model with boundary conditions and specifications as shown in figure 11. The positions of the temperature and heat flux sensor are also shown in the same figure. These are identical to the ones used during the experiments.

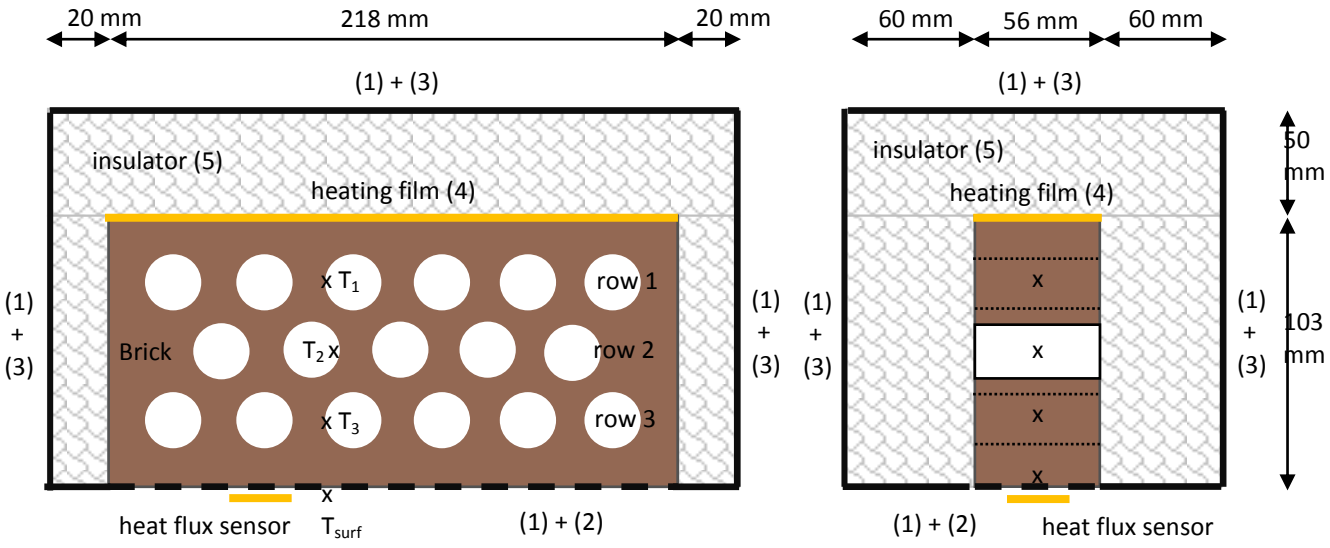

Figure 11: horizontal and vertical cross section through the centre of the tested sample including boundary conditions employed during the simulations.

(1) Convective heat flux boundary: surface heat transfer coefficient calculated by Comsol using "external natural convection" on a "vertical wall" with height of 0.176 m and air as fluid; temperature of surrounding air as measured. In case of top and bottom surfaces "horizontal plate, upside" or "…, downside" were selected.

(2) Surface to ambient radiation boundary: surface emissivity of 0.9; temperature of surrounding air as measured.

(3) Surface to ambient radiation boundary: surface emissivity of 0.8; temperature of surrounding air as measured.

(4) Imposed heat power as source for simulation cases SIM1.x (182 $W.m^{-2}$).

(5) Insulator: thermal conductivity: 0.085 $W.m^{-1}.K^{-1}$; density: 100 $kg.m^{-3}$; specific heat: 1450 $J.kg^{-1}.K^{-1}$. Thermal conductivity was estimated based on the film temperature and insulation surface temperature during the measurement of the bricks with holes filled with solid material.

(*) As initial conditions the measured temperatures of the thermocouples were taken at t=0.

(**) For PCM1, the holes were filled with 102.247 g of PCM. This leads to a volume fraction of PCM of 0.582. For PCM 2 (as a liquid) full filling of the holes was assumed in the simulations.

Table 5 provides an overview of the settings used for the heat transfer in the fluids physics interface; and table 6 for the creeping flow physics interface. For PCM2 these settings were validated in a previous study [22]. Convective heat transfer between the surfaces of the sample and the surrounding environment was calculated by COMSOL, based on specifying the type of heat transfer ("external natural convection" on a "vertical wall", a "horizontal plate, upside" or a "horizontal plate, downside"), the height of the sample (0.176 m) and the type of fluid alongside the sample (air). Radiative heat transfer was calculated by COMSOL, based on specifying the surface emissivity of the materials used (0.9 for the brick and 0.8 for the insulator).

Property setting / value	
Ambient temperature	293.15 K
Ambient abs. pressure	1 atm
Ambient rel. humidity	0
Wind velocity	0 m/s
Initial values	T = 293.15 K

Table 5: settings for the heat transfer in fluids interface.

Property setting / value	
Compressibility	Compressible flow (Ma < 0.3)
Turbulence model	None
Gravity	Included
Reference pressure level	1 atm
Reference temperature	293.15 K
Reference position	x = 0 m; y = 0 m
Initial values	u_x = 0 m/s; u_y = 0 m/s; p = 0 Pa
Compensate for hydrostatic pressure approximation	
Wall conditions	No slip boundary
Neglect internal term (Stokes flow)	

Table 6: settings for the creeping flow interface.

Thermal hysteresis in the enthalpy of the phase change materials was included in the simulations taking the work of Frei [30] and applied by Rubinetti et al. [31], as a starting point but slightly deviating from that. The deviation results from the need to also change between the heating and cooling cycle while the phase change has not been fully completed. A c_p-curve was defined for both the heating and the cooling cycle of the phase change material. The specific heat of the material was then defined as:

$$c_p = (1-f)\cdot c_{p;air} + f\cdot(HorC\cdot c_{p;cooling}(T) + (1-HorC)\cdot c_{p;heating}(T)) \quad [1]$$

in which f denotes the fraction of the holes filled with PCM (the remaining gaps between the PCM granules are filled with air), $c_{p;air}$ [J.kg^{-1}.K^{-1}] is the specific heat of air, $c_{p;cooling}$ [J.kg^{-1}.K^{-1}] is the specific heat of the PCM during the cooling cycle, $c_{p;heating}$ [J.kg^{-1}.K^{-1}] is the specific heat of the PCM during the heating cycle, and *HorC* denotes whether the PCM is cooling down (*HorC* = 1) or heating up (*HorC* = 0).

The variable *HorC* is evaluated at the centroid of every grid element of the phase change material domain. Whether it equals 0 or 1 is defined in de “Domain ODEs and DAEs” interface. Table 7 shows the settings. Important to consider here is the source term. The source term is set-up such that it checks whether the temperature of the centroid of the element during the current time step, T, is higher or lower than the temperature during the previous time step, T_0. If $T < T_0$ then *HorC* = 1; if $T > T_0$ then *HorC* = 0. The nojac-operator is included so that the term behind the operator is not included in the calculation of the Jacobian.

Property	setting / value
Dependent variable quantity	dimensionless
Source term quantity	dimensionless
Shape function type	discontinuous Lagrange
Element order	constant
Frame	spatial
Source term	*HorC*-nojac(if (T<T0,1, if (T>T0,0, *HorC*)))
Damping or Mass Coefficient	0 s
Mass Coefficient	0 s^2
Initial values *HorC*	1 if PCM cools down at the start; else 0
Initial values derivative *HorC*	0

Table 7: settings of the HorC variable in the Domain ODEs and DAEs interface.

The temperature of the previous time step is also defined in the "Domain ODEs and DAEs" interface with table 8 providing the basic settings. Both *HorC* and T_0 are evaluated at previous time steps. This means that they need to be included in the time-dependent solver as previous solution. The *Paradiso solver* of COMSOL was used for the simulations with a relative tolerance set to 0.001. The mesh was set as user-defined with a predefined 'normal' element size calibrated for fluid dynamics, based on a free quad mesh type.

Property	setting / value
Dependent variable quantity	K
Source term quantity	K
Shape function type	Lagrange
Element order	quadratic
Frame	spatial
Source term	T0-nojac(T)
Damping or Mass Coefficient	0 s
Mass Coefficient	0 s^2
Initial values T_0	283
Initial values derivative T_0	0

Table 8: settings of the T_0 variable in the Domain ODEs and DAEs interface

2.4 Part III: wall level simulations: simulation model and settings

Numerical simulations were performed using the COSMOL Multiphysics® Software in order to model the thermal inertia of a complete wall made of BP/S brick with and without PCM. The simulation settings were identical to the settings of the brick-level simulations, except for the geometry of the model and the boundary conditions imposed on the wall.

The simulations of the wall were conducted in 2D instead of 3D. Furthermore, the geometry of the wall was constructed either from one layer or from four layers of three adjacent bricks (see figure 12). The one layer of bricks shows the effects of the individual bricks while the four layers result in a thermal resistance of the brick wall of 4.7 $m^2.K.W^{-1}$, which complies with the current standards for new buildings in the Netherlands and France. An overview of the simulations run are shown in table 9. For most simulations, all 17 holes were filled with identical 'material': air, BP/S, PCM1 or PCM2. However, for 1-layer wall simulations with bricks with PCM2-filled holes also the addition of PCM2 to every row of holes separately was investigated as well.

Hole filling	BP/S	air	PCM1	PCM2
One layer of three adjacent bricks	SIM3.bp/s	SIM3.air	SIM3.pcm1ALL	SIM3.pcm2ALL SIM3.pcm2R1 SIM3.pcm2R2 SIM3.pcm2R3
Four layers of three adjacent bricks	SIM4.bp/s	SIM4.air	SIM4.pcm1ALL	SIM4.pcm2ALL

Table 9: overview of different simulations on wall level.

The boundary condition on the inside includes both convective and IR radiative heat transfer captured in a single surface heat transfer coefficient equal to 7.8 $W.m^{-2}.K^{-1}$ and a fixed indoor air temperature of 20 ^oC. The boundary condition on the outside also includes both convective and IR radiative heat transfer captured in a single surface heat transfer coefficient equal to 25 $W.m^{-2}.K^{-1}$. The outdoor air temperature is based on a sinusoidal function as shown in figure 12. Furthermore, on the outside a general inward heat flux boundary is imposed which mimics solar radiation on the wall surface. The daily radiation on a South façade during end of June / early July on a sunny day in the Netherlands is taken as representative. A Guassian function is used to represent this radiation flux. The albedo of the brick wall was set to 0.2. The combination of the outdoor sinusoidal temperature and the radiation flux on the wall, leads to a temperature of the outdoor surface of the wall shown in figure 13. As initial condition regarding the temperature of the wall, 20 ^oC was used. Finally, a "normal" physics-controlled mesh

element size was set. And the simulations covered a time frame of 7 days for the walls with one layer of bricks and 28 days for the walls with four layers of bricks.

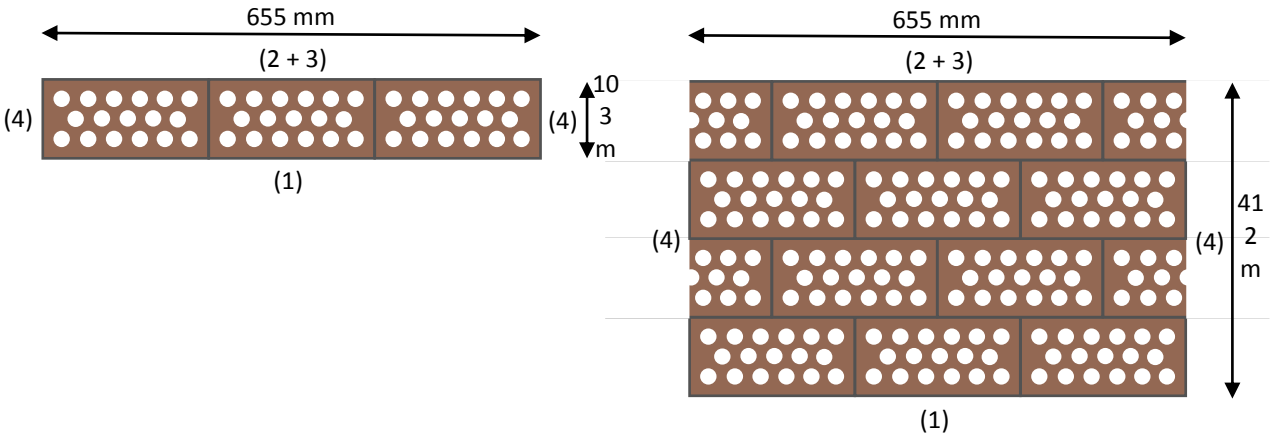

Figure 12: horizontal cross section through the simulated part of the brick wall (left: one layer; right: four layers) including boundary conditions employed during the simulations.

(1) Convective heat flux boundary: surface heat transfer coefficient equal to 7.8 $W.m^{-2}.K^{-1}$; fixed surrounding air temperature at 20 ^{o}C.

*(2) Convective heat flux boundary: surface heat transfer coefficient equal to 25 $W.m^{-2}.K^{-1}$; sinusoidal surrounding air temperature: T = 25+10*sin(2*pi/86400*t-2*pi/3)).*

*(3) General inward heat flux boundary (repeated for every simulation day): q_0 $[W.m^{-2}]$ = (1-albedo)*2900/(2.6*sqrt(2*pi))*exp(-((t/3600-13.45)^2)/(2*2.6^2)); albedo = 0.2. This boundary condition mimics the impact of solar radiation.*

(4) Adiabatic boundary.

(**) For PCM1, the holes were filled with 102.247 g of PCM. This leads to a volume fraction of PCM of 0.582. For PCM 2 (as a liquid) full filling of the holes was assumed in the simulations.

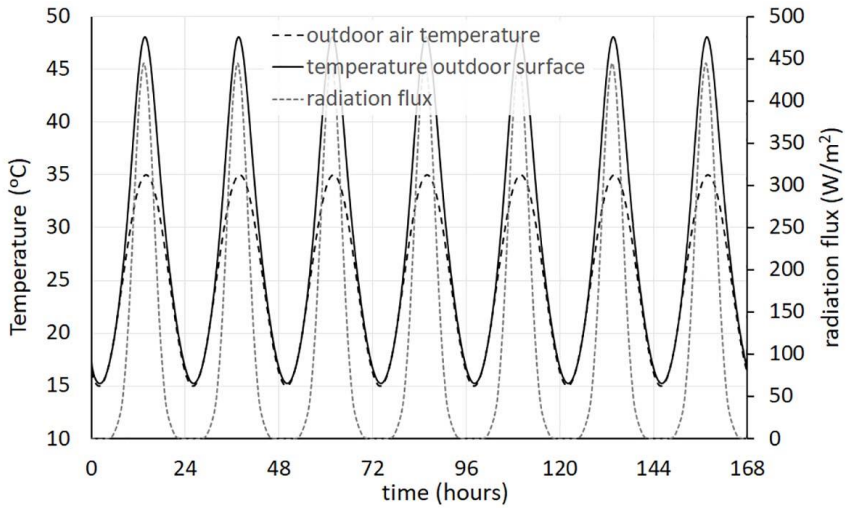

Figure 13: outdoor air temperature and radiation flux as input for the simulation model, and simulated temperature of the outdoor surface of the wall with one layer of bricks with air-filled holes.

3. Results and discussion of the experimental measurements

3.1 Heating the brick

Figure 14 shows the results of the measurements on the different brick specimens that were heated by a heating film (25 V, 89 mA). Because not all bricks start cooling down from the same temperature, figure 15 shows normalized graphs in which the measured temperature is divided by the measured maximum temperature of the respective thermocouple. These normalized graphs allow for a better comparison of the impact of the thermal inertia on the cooling process. It is important to note that the time the heating film was switched on was not the same for every case tested.

As can be observed from the graphs, during heating the time constants are different. The changes of the temperatures in the case of the bricks with PCM-filled holes are slower than the changes in the case of the other two bricks. Furthermore, the temperature changes in the bricks with BP/S-filled holes are slightly slower than in the bricks with air-filled holes. This shows that the PCM inside the holes increases the thermal inertia of the bricks.

Furthermore, the temperatures in the case of PCM-filled holes also are higher once steady-state has been reached than those in the solid brick or brick with holes filled with air.

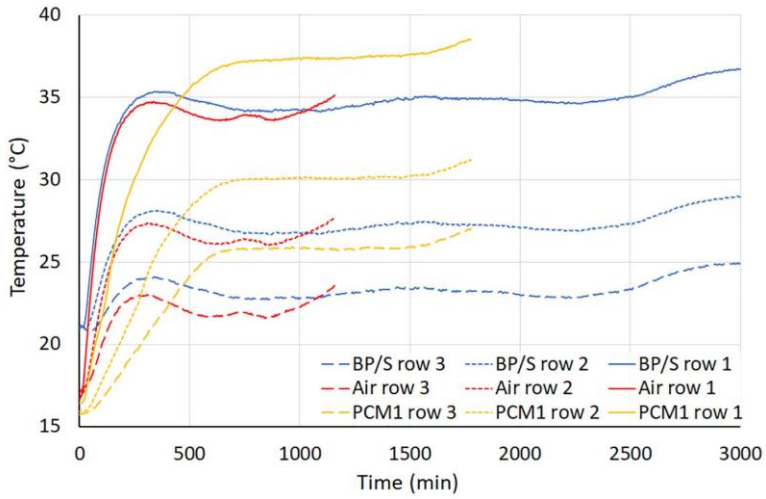

Figure 14: comparison of the results of the measured temperatures inside the holes in rows 1, 2 and 3 for the bricks with holes filled with BP/S, air and PCM1 respectively. Heating mode.

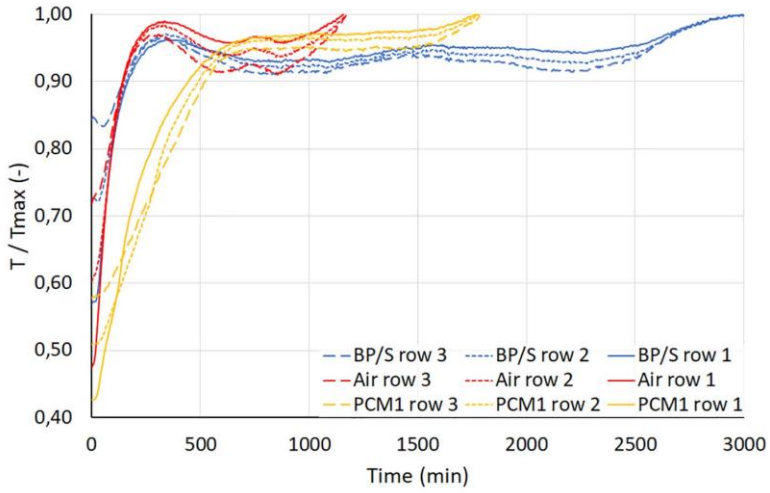

Figure 15: comparison of the results of the measured temperatures inside the holes in rows 1, 2 and 3 for the bricks with holes filled with BP/S, air and PCM1 respectively, normalised to the maximum temperature. Heating mode.

3.2 Passively cooling down the brick

Figure 16 shows the results of the measurements on the various brick specimens that were passively cooling down. Normalized graphs are also presented here for better comparison of the thermal inertia (figure 17). As can be seen from the graphs, the time constants are also different during passive cooling. Again, the changes of the temperatures in the case of the bricks with PCM-filled holes are slower than the changes in the case of the other two bricks. Furthermore, the temperature changes in the bricks with BP/S-filled holes are again slower than in the bricks with air-filled holes. This supports the previous results that the PCM inside the holes increases the thermal inertia of the bricks.

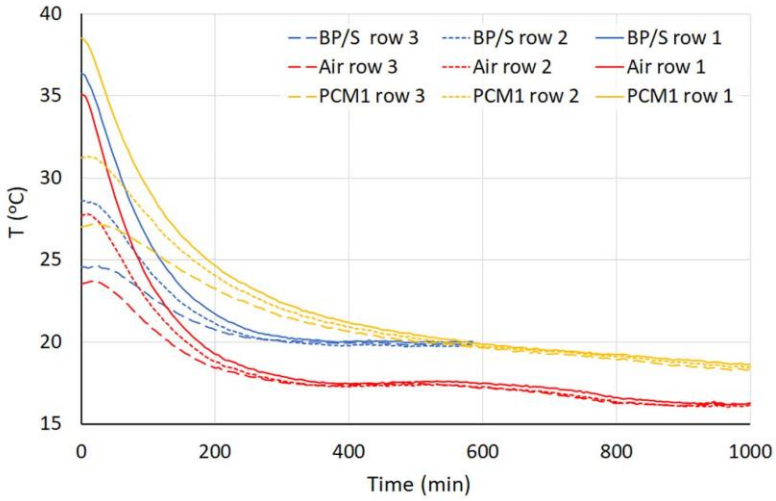

Figure 16: comparison of the results of the measured temperatures inside the holes in rows 1, 2 and 3 for the bricks with holes filled with BP/S, air and PCM1 respectively. Cooling down mode.

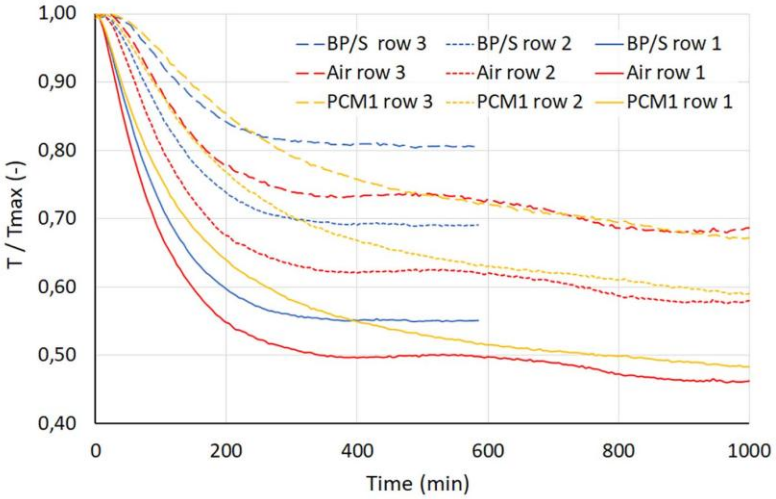

Figure 17: comparison of the results of the measured temperatures inside the holes in rows 1, 2 and 3 for the bricks with holes filled with BP/S, air and PCM1 respectively, normalised to the maximum temperature. Cooling down mode.

4. **Results and discussion of the simulations**

4.1 Heating the brick

Figure 18 presents the results of the simulations in comparison to the results of the measurements. As can be seen from the results, there is in general good agreement between the measurements and the simulations. The normalised root mean square error (normalised RMSE) for the bricks with holes filled with BP/S, air and PCM1 respectively are presented in table 10. The thermocouple used in the

experiments in the row of holes closest to the surface (row 3) gives the highest difference between experimental measurements and simulations, especially in the case BP/S-filled holes. This could be explained if the thermocouple slightly moved position during the filling of the holes. In general, these results support the conclusions from the experiments that the PCM inside the holes increases the thermal inertia of the bricks.

In addition, figure 18 also shows the simulated results of bricks with PCM2-filled holes with a higher latent heat of fusion. As can be seen, the PCM2-filled bricks even have a higher thermal inertia than the ones filled with PCM1. This is in line with the c_p values used as input for the simulations. The results of the latent heat of fusion are more clearly visible for PCM2 as abrupt changes in the temperature evolution.

According to the simulations, the change in total enthalpy of the different entire bricks (from initial conditions to end conditions) equals 11.3 $kJ.kg^{-1}$ for the BP/S-filled brick, 14.5 $kJ.kg^{-1}$ for the air-filled brick, 28.9 $kJ.kg^{-1}$ for the PCM1-filled brick and 37.4 $kJ.kg^{-1}$ for the PCM2-filled brick. When considering these results, it is important to observe that the brick with PCM2 has not yet reached its maximum steady state temperature; and that the brick with BP/S filled holes reached a lower maximum temperature than the air-filled brick. These results support the previous observations regarding thermal inertia of the various bricks.

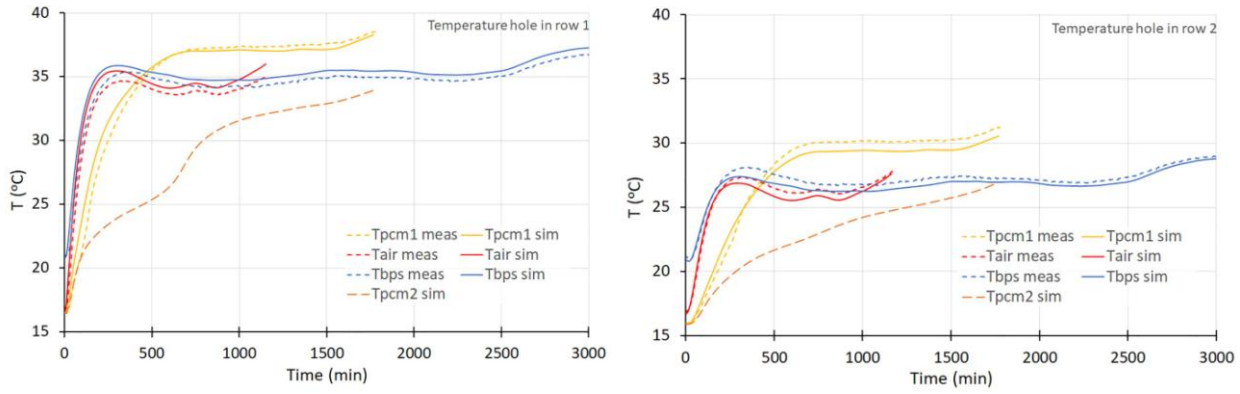

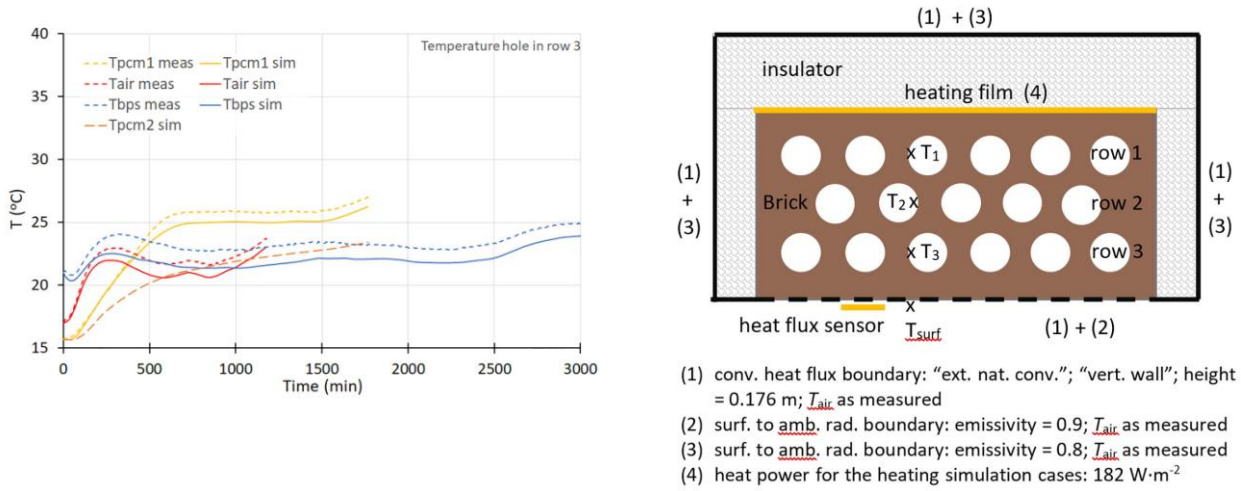

Figure 18: comparison of the results of the simulation to the results of the measurements for the bricks filled with BP/S, air, PCM1 and PCM2 (only simulations). Top left: the temperature inside the hole in row 1; Top right: the temperature inside the hole in row 2; Bottom: the temperature inside the hole in row 3. Heating mode.

	Row 1	Row 2	Row 3
Holes filled with BP/S	0.041	0.051	0.298
Holes filled with Air	0.051	0.039	0.139
Holes filled with PCM1	0.036	0.044	0.064

Table 10: Normalised root mean square error for the temperature during the heating/relaxing mode simulations.

Figure 19 shows the heat flux density on the surface of the brick exposed to the ambient air. As can be seen, large differences between the simulations and the measurements appear for all the cases studied. In the simulation model, the convective surface heat transfer coefficient was modelled based on free convection. However, it is likely that more air movement along the surface was present during the experimental measurements, which increases the convective surface heat transfer coefficient considerably.

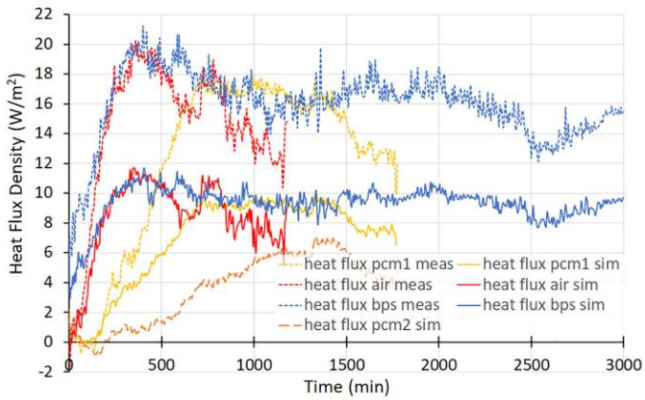

Figure 19: comparison of the results of the simulation to the results of the measurements for the bricks filled with BP/S, air, PCM1 and PCM2 (only simulations). Heat flux density from the front surface to the surrounding air is plotted. Heating mode.

4.2 Passively cooling down the brick

Figure 20 presents the results of the simulations in comparison to the results of the measurements for the case of passively cooling down the bricks. As can be seen from the results, also here in general there is good agreement between the measurements and the simulations. The normalised root mean square error (normalised RMSE) for the bricks with holes filled with BP/S, air and PCM1 respectively are presented in table 11. The results of the simulations therefore support the conclusions from the experimental measurements that the PCM inside the holes increases the thermal inertia of the bricks.

In addition, figure 20 also shows the simulated results of bricks in which the holes are filled with PCM2 have a higher latent heat of fusion. As can be seen, the bricks with holes filled with PCM2 also here show a higher thermal inertia, however in a smaller temperature range than the ones filled with PCM1. It is important to note that the initial temperature of the bricks of which the holes are filled with PCM2 is lower than of the one filled with PCM1. The reason is that during the heating process (before the cooling process commenced) the temperature of the PCM2 did not reach a steady-state situation when the heating power of the heating film was switched off; hence, a lower initial temperature.

According to the simulations, the change in total enthalpy of the different entire bricks (from initial conditions to end conditions) equals -11.9 $kJ.kg^{-1}$ for the BP/S-filled brick, -15.7 $kJ.kg^{-1}$ for the air-filled brick, -27.5 $kJ.kg^{-1}$ for the PCM1-filled brick and -21.0 $kJ.kg^{-1}$ for the PCM2-filled brick. Regarding the PCM2-filled brick, it is interesting to note that the material is still in its process of phase change and the temperature drop has been small. These results support the previous observations regarding thermal inertia of the different bricks.

Figure 21 shows the heat flux density on the surface of the brick exposed to the ambient air. It has to be noted here that the heat flux density is generally larger in the case of the experimental measurements as compared to the simulations.

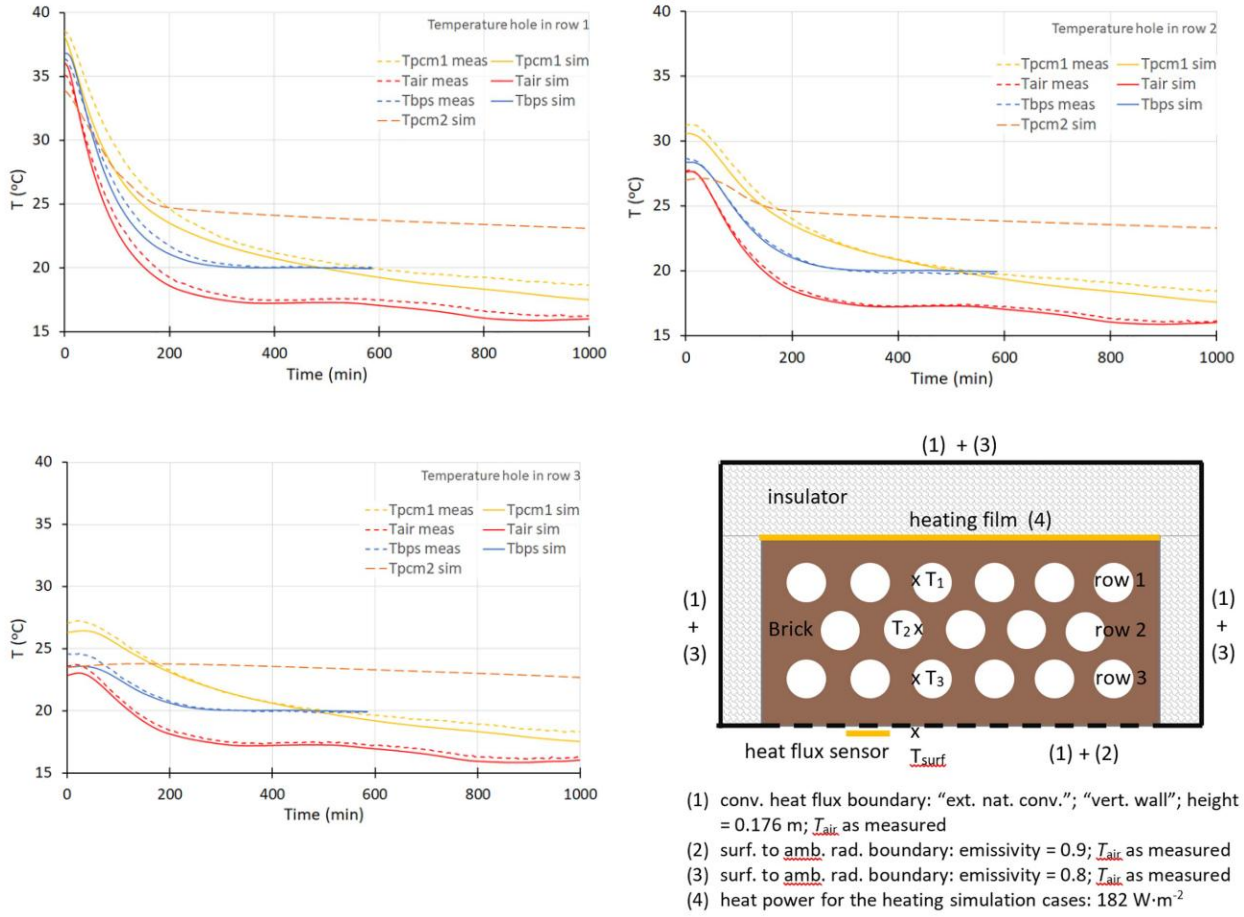

Figure 20: comparison of the results of the simulation to the results of the measurements for the bricks filled with BP/S, air, PCM1 and PCM2 (only simulations). Top left: the temperature inside the hole in row 1; Top right: the temperature inside the hole in row 2; bottom: the temperature inside the hole in row 3. Cooling down mode.

	Row 1	Row 2	Row 3
Holes filled with BP/S	0.029	0.017	0.073
Holes filled with Air	0.026	0.019	0.041
Holes filled with PCM1	0.046	0.046	0.061

Table 11: Normalised root mean square error for the temperature during the cooling down mode simulations.

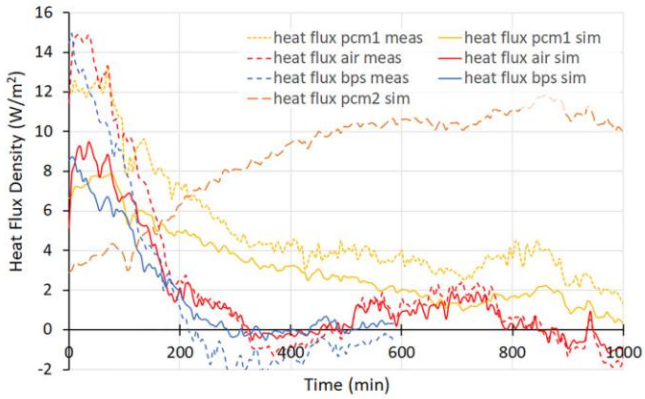

Figure 21: comparison of the results of the simulation to the results of the measurements for the bricks filled with BP/S, air, PCM1 and PCM2 (only simulations). Heat flux density from the front surface to the surrounding air is plotted. Cooling down mode.

4.3 Wall level simulations with sinusoidal temperature and radiation flux excitation

Figures 22, 23 and 24 show the indoor surface temperature of the 1-layer brick wall respectively the 4-layer brick wall, for the four different variants of hole filling: air, BP/S, PCM1 and PCM2 (ALL, Layer1, Layer2, Layer3). As can be seen, adding PCM to all the holes enlarges the thermal inertia of the brick wall, especially in the case of the 1-layer wall filled with PCM2. The temperature amplitude damping on the indoor surface is high. For the 4-layer wall, the PCM does increase the thermal inertia but since the bricks themselves already have high thermal inertia the additional effect is still present but has lower practical value.

Tables 12 and 13 present an overview of the temperature amplitude damping and the phase shift relative to when the temperature peak on the external surface appears. These results show that the temperature amplitude on the indoor surface of the 1-layer brick wall changes from 1.12 ^{o}C and 1.18 ^{o}C for the bricks with holes filled with BP/S and air, to 0.95 ^{o}C and 0.03 ^{o}C for the bricks with holes filled with PCM1ALL and PCM2ALL. The large difference between the performance of PCM1 and PCM2 can be explained by two reasons. First, the latent heat of fusion of PCM1 is smaller than of PCM2. Second, the average PCM temperature of all PCM inside the brick wall on the 6th day during all 24 hours is equal to 24.3 ^{o}C (with an amplitude of 6.0 ^{o}C) for PCM1 and to 23.9 ^{o}C (with an amplitude of 1.3 ^{o}C) for PCM2. For PCM1 this temperature fluctuation is for a large part outside the active temperature range of the material whilst for PCM2 it more closely matches with the active temperature range. Also, the phase shift of the temperature peaks on the indoor surface as compared to the outdoor surface clearly show the effect of the added thermal inertia (see also figure 25).

Regarding the position of the PCM, figures 23 and 25 and table 12 show that PCM placed closest to the outdoor or indoor surface gives a higher temperature amplitude damping on the indoor surface than PCM placed in the centre of the brick wall. Also the time delay is longer. Comparing these two positions,

the PCM placed in the holes closest to the outdoor surface (row 1) leads to a lower indoor surface as compared to placing the PCM close to the indoor surface (row 3). Under warm summer conditions, a cooler indoor surface would be preferred, and thus placement of the PCM in row 1.

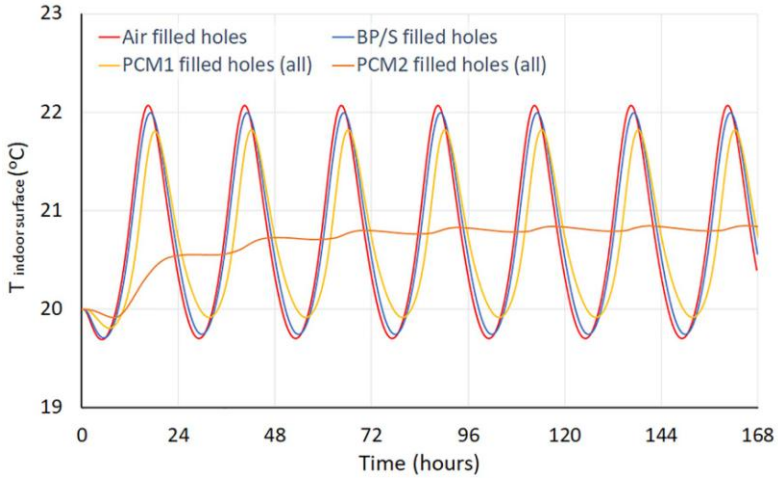

Figure 22: simulated temperature evolution of the indoor surface of the 1-layer brick wall filled with BP/S, air, PCM1 and PCM2, exposed to an outdoor temperature fluctuation and an outdoor radiation flux.

Figure 23: simulated temperature evolution of the indoor surface of the 1-layer brick wall filled with PCM2 (all, row1, row2 or row3), exposed to an outdoor temperature fluctuation and an outdoor radiation flux.

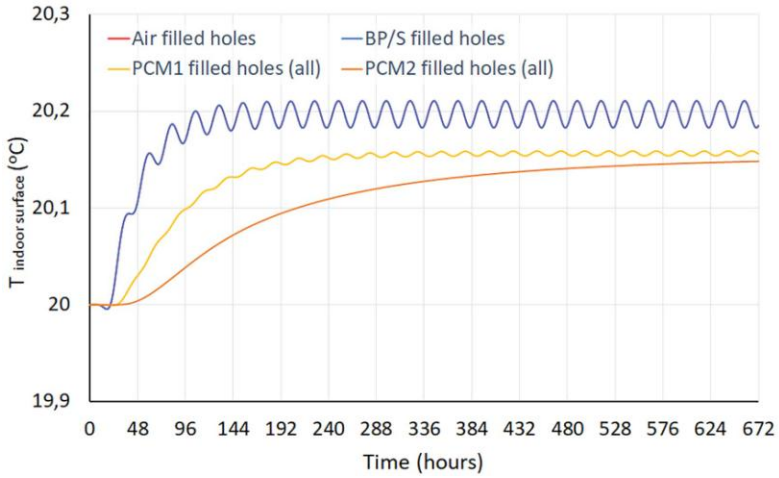

Figure 24: simulated temperature evolution of the indoor surface of the 4-layer brick wall filled with BP/S, air, PCM1 and PCM2, exposed to an outdoor temperature fluctuation and an outdoor radiation flux. The results for BP/S-filled holes (blue line) almost entirely overlap the results for air-filled holes (red line) in the graph.

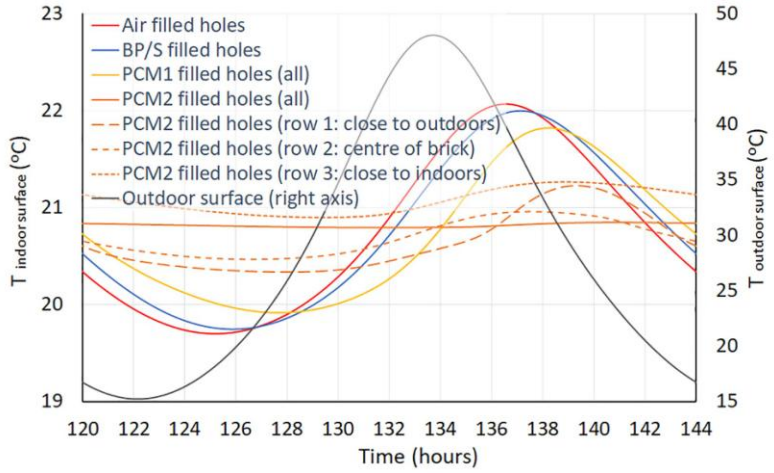

Figure 25: simulated temperature evolution of the indoor surface of the 1-layer brick wall filled with BP/S, air, PCM1 and PCM2 (different configurations), exposed to an outdoor temperature fluctuation and an outdoor radiation flux. Results only for day 6. Outdoor surface temperature is plotted on the y-axis on the right side of the figure.

1-layer brick wall	Temperature amplitude indoor surface (max; min) [°C]	Temperature amplitude damping indoor surface [°C]	Phase shift of the temperature on the indoor surface [h]
Holes filled with BP/S	1.12 (22.00; 19.75)	0.069	3.3
Holes filled with Air	1.18 (22.07; 19.70)	0.072	2.8
Holes filled with PCM1	0.95 (21.82; 19.92)	0.059	4.5
Holes filled with PCM2 (all rows)	0.03 (20.85; 20.80)	0.002	7.3

Holes filled with PCM2 (row 1: close to outdoors)	0.45 (21.23; 20.34)	0.015	5.7
Holes filled with PCM2 (row 2: centre of brick)	0.25 (20.96; 20.47)	0.008	3.8
Holes filled with PCM2 (row 3: close to indoors)	0.18 (21.27; 20.90)	0.006	5.3

Table 12: overview of the temperature amplitude, temperature amplitude damping (= temp. amplitude indoor surface / temp. amplitude outdoor surface) and the phase shift of the temperature on the indoor surface as compared to the temperature on the outdoor surface of the 7 simulated variants of the 1-layer brick wall (based on last complete cycle).

4-layer brick wall	Temperature amplitude indoor surface (max; min) [^{o}C]	Temperature amplitude damping indoor surface [^{o}C]	Phase shift of the temperature on the indoor surface [h]
Holes filled with BP/S	0.01 (20.21; 20.18)	0.001	20.2
Holes filled with Air	0.01 (20.21; 20.18)	0.001	20.2
Holes filled with PCM1	0.00 (20.14; 20.13)	0.000	30.2
Holes filled with PCM2 (all rows)	0.00 (20.08; 20.07)	0.000	> 40

Table 13: overview of the temperature amplitude, temperature amplitude damping (= temp. amplitude indoor surface / temp. amplitude outdoor surface) and the phase shift of the temperature on the indoor surface as compared to the temperature on the outdoor surface of the 4 simulated variants of the 4-layer brick wall (based on last complete cycle).

5. Conclusions

Due to environmental concerns, bio-based materials are becoming increasingly investigated. Besides, their application in buildings is on the rise too. Bio-based materials can have beneficial properties regarding their low environmental impact. However, the density of these materials is low, and as a result, they possess a low thermal inertia. High thermal inertia can be beneficial for reducing the energy use of building by damping indoor temperature fluctuations or by reducing and delaying incoming (solar) heat through the façade.

This study investigated the thermal inertia of bio-sourced bricks (218 mm x 103 mm x 56 mm) made of a sugar-beet-pulp and starch composite (BP/S). Inside the bricks, 17 holes (in three rows) with a radius of 8.5 mm were present to improve insulation properties and reduce the amount of material used. The holes were filled either with the BP/S mixture, with air or with a phase change material (PCM). Two types of PCM were explored in order to investigate to what extent a PCM can increase the thermal inertia of the brick. The brick was insulated on all sides but one. Two series of experimental measurements were performed: 1.) a heating film placed at the back (insulated) side of the brick heated

the brick until steady-state conditions were reached; 2.) the heated brick was then passively cooled down to ambient temperature by cutting the power to the heating film. The temperatures inside and around the brick were monitored with thermocouples and the heat flux density from the surface to the ambient was monitored using heat flux sensors. These experimental measurements were also reproduced using direct numerical simulations modelled using the COMSOL Multiphysics® Software. In addition, simulations were run to study the thermal inertia of a full brick wall made out of 1 layer and of 4 layers of the BP/S brick with and without PCM, exposed to a combination of a sinusoidal outdoor air temperature fluctuation with an imposed radiation flux on the outdoor surface, representing summer conditions.

The results show that it is possible to accurately reproduce the measurements with the simulations. Furthermore, both the measurements and the simulations show that the bricks of which the holes were filled with phase change material had a slower temperature response, and thus a higher thermal inertia, than the bricks of which the holes were filled with BP/S or with air. The salt-hydrate based PCM (PCM2) with higher latent heat of fusion led to the slowest temperature response and highest thermal inertia. Moreover, simulations on wall level confirmed the additional thermal inertia induced by the PCM, showing that the temperature amplitude on the indoor surface of a 1-layer brick wall reduced from 1.18^{o}C for bricks with air-filled holes to 0.95 ^{o}C and 0.03 ^{o}C for bricks with PCM1- resp. PCM2-filled holes. PCM2 outperformed PCM1 because of its higher latent heat of fusion and of the better match between the occurring temperature range and its active temperature range. Furthermore, the wall level simulations showed that the added effect of the PCM to a 4-layer brick wall did to have significance for practice. Regarding the position of the PCM inside the brick wall, under warm summer conditions, placing it closest to the outdoor surface leads to a high temperature amplitude damping and the lowest indoor surface temperature among the tested variants. Embedding PCM inside lightweight bio-sourced construction materials may therefore increase the application potential of such materials, especially in case of relatively thin walls.

Future work will focus on evaluating the effect of walls on building level under real climatic conditions and with different ventilation systems, as well as assessing environmental benefits of bio-based bricks especially regarding their carbon reduction potential when used as building material.

Funding

This work was made possible through a grant in the framework of the van Gogh programme, which is a joint initiative of the Dutch organisation Nuffic and the French organisation Campus France [grant number: NL: VGP.18/00005 CF103229; F: 42530UJ].

References

[1] Eurostat, Final Energy Consumption by Sector. https://ec.europa.eu/eurostat/databrowser/view/ten00124/default/table?lang=en, 2022 (accessed 21 July 2022.

[2] J.F. Azcarate-Aguerre, M. Conci, M. Zils, P. Hopkinson, T. Klein, 2022. Building energy retrofit-as-a-service: a Total Value of Ownership assessment methodology to support whole life-cycle building circularity and decarbonisation. Construction Management and Economics. 40 (9). https://doi.org/10.1080/01446193.2022.2094434.

[3] European Commission, Closing the loop: Commission delivers on Circular Economy Action Plan. http://europa.eu/rapid/pressrelease_IP-19-1480_en.html, 2019 (accessed 21 July 2022).

[4] Ellen MacArthur Foundation, The butterfly diagram: visualising the circular economy. https://ellenmacarthurfoundation.org/circular-economy-diagram, 2019 (accessed 21 July 2022).

[5] C. Maalouf, A.D.T. Le, S.B. Umurigirwa, M. Lachi, O. Douzane, 2014. Study of hygrothermal behavior of a hemp concrete building envelope under summer conditions in France. Energy and Buildings. 77. https://doi.org/10.1016/j.enbuild.2014.03.040.

[6] F. Collet, S. Pretot, 2014. Thermal conductivity of hemp concretes: variation with formulation, density and water content. Construction and Building Materials. 65. https://doi.org/10.1016/j.conbuildmat.2014.05.039.

[7] T. Colinart, D. Lelievre, P. Glouannec, 2016. Experimental and numerical analysis of the transient hygrothermal behavior of multilayered hemp concrete wall. Energy and Buildings. 112. https://doi.org/10.1016/j.enbuild.2015.11.027.

[8] B. Haba, B. Agoudjil, A. Boudenne, K. Benzarti, 2017. Hygric properties and thermal conductivity of a new insulation material for building based on date palm concrete. Construction and Building Materials. 154. https://doi.org/10.1016/j.conbuildmat.2017.08.025.

[9] H. Karaky, C. Maalouf, C. Bliard, T. Moussa, N. El Wakil, M. Lachi, G. Polidori, 2018. Hygrothermal and Acoustical Performance of Starch-Beet Pulp Composites for Building Thermal Insulation. Materials. 11, 1622. https://doi.org/10.3390/ma11091622.

[10] H. Karaky, C. Maalouf, C. Bliard, A. Gacoin, M. Lachi, N. El Wakil, G. Polidori, 2019. Characterization of beet-pulp fiber reinforced potato starch biopolymer composites for building applications. Construction and Building Materials. 203, 01.127. https://doi.org/10.1016/j.conbuildmat.2019.01.127.

[11] G. Constantine, E. Harb, C. Bliard, C. Maalouf, E. Kinab, B. Abbes, F. Beaumont, G. Polidori, 2020. Experimental characterization of starch/beet-pulp bricks for building applications: drying kinetics and mechanical behavior. Construction and Building Materials. 264, 120270. https://doi.org/10.1016/j.conbuildmat.2020.120270.

[12] J.M. Gutherz, M.E. Schiler, 1991. A passive solar heating system for the perimeter zone of office buildings. Energy Sources. 13. https://doi.org/10.1080/00908319108908967.

[13] H. Weinläder, A. Beck, J. Fricke, 2005. PCM-façade-panel for daylighting and room heating. Solar Energy. 78 (2). https://doi.org/10.1016/j.solener.2004.04.013.

[14] F. Goia, M. Perino, V. Serra, 2013. Improving thermal comfort conditions by means of PCM glazing systems. Energy and Buildings. 60. https://doi.org/10.1016/j.enbuild.2013.01.029.

[15] V.V. Tyagi, D. Buddhi, 2007. PCM thermal storage in buildings: A state of art. Renewable and Sustainable Energy Reviews. 11 (6). https://doi.org/10.1016/j.rser.2005.10.002.

[16] R. Baetens, B.P. Jelle, A. Gustavsen, 2010. Phase change materials for building applications: A state-of-the-art review. Energy and Buildings. 42 (9). https://doi.org/10.1016/j.enbuild.2010.03.026.

[17] S.E. Kalnaes, B.P. Jelle, 2015. Phase change materials and products for building applications: A state-of-the-art review and future research opportunities. Energy and Buildings. 94. https://doi.org/10.1016/j.enbuild.2015.02.023.

[18] A. Bland, M. Khzouz, T. Statheros, E.I. Gkanas, 2017. PCMs for residential building applications: A short review focussed on disadvantages and proposals for future development. Buildings. 7 (3), 78. https://doi.org/10.3390/buildings7030078.

[19] F. Fiorito, 2012. Trombe walls for lightweight buildings in temperate and hot climates. Exploring the use of pcms for performance improvement. Energy Proceedia. 30. https://doi.org/10.1016/j.egypro.2012.11.124.

[20] Q. Wang, C.Y. Zhao, 2015. Parametric investigations of using PCM curtain for energy efficient buildings. Energy and Buildings. 94. https://doi.org/10.1016/j.enbuild.2015.02.024.

[21] M. Tenpierik, M. Turrin, Y. Wattez, T. Cosmatu, S. Tsafou, 2018. Double Face 2.0: A lightweight translucent adaptable Trombe wall. SPOOL. 5 (2, Expo #1). https://doi.org/10.7480/spool.2018.2.2090.

[22] M. Tenpierik, Y. Wattez, M. Turrin, T. Cosmatu, S. Tsafou, 2019. Temperature Control in (Translucent) Phase Change Materials Applied in Facades: A Numerical Study. Energies. 12 (17), 3286. https://doi.org/10.3390/en12173286.

[23] X. Wang, H. Yu, L. Li, M. Zhao, 2016. Experimental assessment on the use of phase change materials (PCMs)-bricks in the exterior wall of a full-scale room. Energy Conversion and Management. 120. https://doi.org/10.1016/j.enconman.2016.04.065.[24] A. Laaouatni, N. Martaj, R. Bennacer, M. El Omari, M. El Ganaoui, 2017. Phase change materials for improving the building thermal inertia. Energy Proceedia. 139. https://doi.org/10.1016/j.egypro.2017.11.281.

[25] A. Laaouatni, N. Martaj, R. Bennacer, M. Lachi, M. El Omari, M. El Ganaoui, 2019. Thermal building control using active ventilated block integrating phase change material. Energy and Buildings. 187. https://doi.org/10.1016/j.enbuild.2019.01.024.

[26] M. Sawadogo, F. Benmahiddine, A. El Amine Hamami, R. Belarbi, A. Godin, M. Duquesne, 2022. Investigation of a novel bio-based phase change material hemp concrete for passive energy storage in buildings. Applied Thermal Engineering. 212, 118620. https://doi.org/10.1016/j.applthermaleng.2022.118620.

[27] D.S. Canim, S.M. Kalfa, 2023. Development of a new pumice block with phase change material as a building envelope component. Journal of Energy Storage. 61, 106706. https://doi.org/10.1016/j.est.2023.106706.

[28] E. Alayed, D. Bensaid, R. O'Hegarty, O. Kinnane, 2022. Thermal mass impact on energy consumption for buildings in hot climates: A novel finite element modelling study comparing building constructions for arid climates in Saudi Arabia. Energy and Buildings. 271, 112324. https://doi.org/10.1016/j.enbuild.2022.112324.

[29] H. Johra, P. Heiselberg, J. Le Dréau, 2019. Influence of envelope, structural thermal mass and indoor content on the building heating energy flexibility. Energy and Buildings. 183. https://doi.org/10.1016/j.enbuild.2018.11.012.

[30] W. Frei, Thermal Modeling of Phase-Change Materials with Hysteresis. https://www.comsol.com/blogs/thermal-modeling-of-phase-change-materials-with-hysteresis/?msclkid=21330513a9e711ec817c0cea6736cc0c, 2016 (accessed 21 July 2022).

[31] D. Rubinetti, D.A. Weiss, D. Kraniotis, A. Chaudhuri, 2020. Fully integrated numerical design tool to assess the thermal performance of phase change materials (PCM) in the built environment. IOP Conf. Ser.: Earth and Environmental Science. 410, 012114. https://doi.org/10.1088/1755-1315/410/1/012114.